

## Article

# Provenance Tracing and Age Analysis of Lead–Zinc Mineralization in Qiyimuchang, Inner Mongolia, NE China

Mingxin Duan <sup>1,2</sup>, Yunsheng Ren <sup>3,\*</sup>, Chunji Xue <sup>1</sup>, Qun Yang <sup>3</sup>, Yujie Hao <sup>3</sup> and Tao Liu <sup>2</sup><sup>1</sup> School of Earth Sciences and Resources, China University of Geosciences (Beijing), Beijing 100083, China<sup>2</sup> Harbin Center for Integrated Natural Resources Survey, China Geological Survey, Harbin 150086, China<sup>3</sup> College of Earth Sciences, Jilin University, Changchun 130061, China

\* Correspondence: author: renys@jlu.edu.cn

**Abstract:** The Qiyimuchang lead–zinc deposit is an important deposit in the Erguna Massif on the west slope of Daxinganling, for which the material source and age of mineralization remain unclear. The lead–zinc deposit in Qiyimuchang has been observed to occur in Jurassic volcanic strata as a vein-like orebody, and its strike is nearly perpendicular to that of the strata and the regional structures of the orogenic belt. The ore is mainly composed of sphalerite, galena, chalcopryrite, pyrite, and quartz, and hydrothermal alteration zones dominated by silicification, fluoritization, and pyritization are common within 1–5 m on both sides of the vein. The metasomatic lead–zinc mineralization is characterized by a massive vein structure. The mineralization process can be divided into three stages, pre-ore (mainly quartz, arsenopyrite and a small amount of pyrite), ore-formation (pyrite, chalcopryrite, sphalerite, galena, fluorite, and a small amount of tetrahedrite), and post-ore (quartz-calcite veinlets with a small amount of pyrite). Element and isotope geochemical studies show that the trace element compositions of the wall rocks (andesite, tuff, etc.) of Jurassic volcanic rocks in the ore bodies and surrounding rocks reflect affinity or similarity between them. The S isotopic composition of sulfide minerals in the metallogenic stage ( $\delta^{34}\text{S}_{\text{V-CDT}} = 1.6\text{‰} \sim 4.8\text{‰}$ ) indicate the sulfur isotopic composition of the magma. The Pb isotopic compositions of sulfide minerals (38.5–38.39, 15.55–15.62, and 18.33–18.41 for  $^{208}\text{Pb}/^{204}\text{Pb}$ ,  $^{207}\text{Pb}/^{204}\text{Pb}$ , and  $^{206}\text{Pb}/^{204}\text{Pb}$ , respectively) in the metallogenic stage are relatively concentrated and close to the average Pb isotopic compositions of the mantle and average Pb isotopic composition of an orogenic belt, indicating that the ore-forming metals are likely to be a mixed source of crust and mantle. A new zircon U–Pb age of  $150.8 \pm 1.3$  Ma (MSWD = 0.74) was obtained from andesitic tuff. Collectively considering the regional geology and ore deposit geological analysis, the lead–zinc mineralization in Qiyimuchang possibly occurred during the early Cretaceous. The ore-forming processes belong to Cretaceous magmatic-hydrothermal activity in extensional tectonic setting.



**Citation:** Duan, M.; Ren, Y.; Xue, C.; Yang, Q.; Hao, Y.; Liu, T. Provenance Tracing and Age Analysis of Lead–Zinc Mineralization in Qiyimuchang, Inner Mongolia, NE China. *Minerals* **2022**, *12*, 1146. <https://doi.org/10.3390/min12091146>

Academic Editor: Georgia Pe-Piper

Received: 11 August 2022

Accepted: 9 September 2022

Published: 10 September 2022

**Publisher's Note:** MDPI stays neutral with regard to jurisdictional claims in published maps and institutional affiliations.



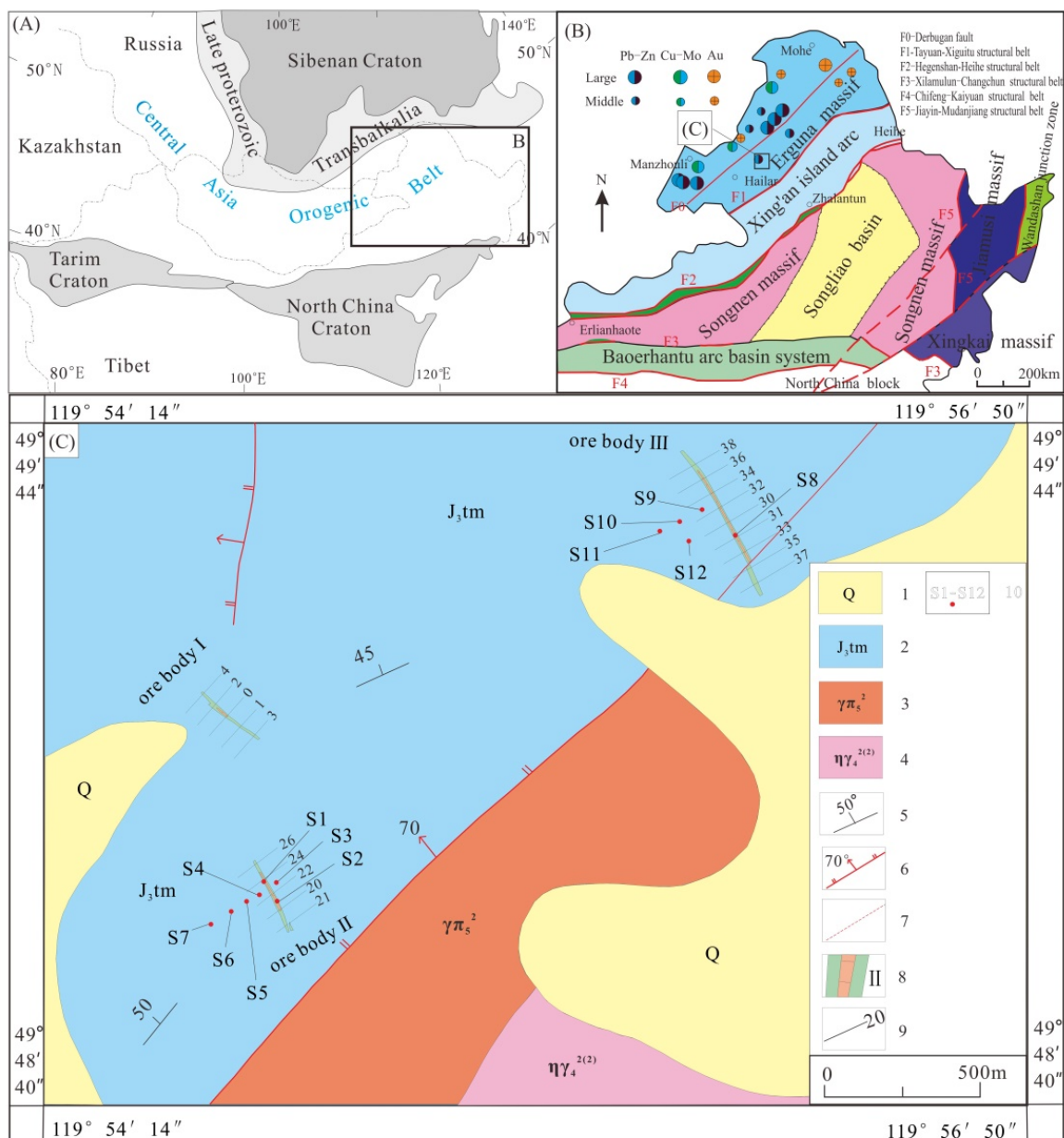
**Copyright:** © 2022 by the authors. Licensee MDPI, Basel, Switzerland. This article is an open access article distributed under the terms and conditions of the Creative Commons Attribution (CC BY) license (<https://creativecommons.org/licenses/by/4.0/>).

**Keywords:** Qiyimuchang lead–zinc deposit; geochemistry; S–Pb isotope; zircon U–Pb geochronology

## 1. Introduction

The Erguna Massif is located in the eastern section of the Xing'an–Mongolia orogenic belt in the east of the Central Asia Orogenic Belt (CAOB) (Figure 1A). Prospecting and exploration activities have revealed a large amount of lead–zinc (silver) deposits in this area (Figure 1B), with many large-size deposits, such as the Jiawula large-size lead–zinc (silver) deposit (lead and zinc resources of more than 1.3 million tons), E'rentaolegai large-size silver and manganese deposit, large-size lead–zinc (silver) deposits in Biliyagu (more than 0.7 million tons), and large-size lead–zinc deposits in Derbur (more than 1.1 million tons) [1–5]. The extensive lead–zinc mineralization in the Erguna Massif has attracted much attention [6–9]. The lead–zinc deposits in the area are distributed belt-like along the NNE, striking the Derbugan fault, and most of them exist as veins in Mesozoic volcanic rocks. Thus far, most studies on these deposits have focused on the western part of the

Derbugan fault, and the newly discovered lead–zinc deposits in the east of the fault, such as the Qiyimuchang lead–zinc deposit and Dongjun lead–zinc deposit, was poorly studied. Varied conclusions have been drawn regarding the source of the ore-forming materials, such as crust mantle mixed source [1,2,4], crust mantle mixed source dominated by mantle source [10,11], and upper crust [12,13]. Moreover, their mineralization and ore controlling elements are poorly understood.



**Figure 1.** Geotectonic location map ((A) after [14]; (B) modified by [15]) and geological map ((C) after [16]) of the Qiyimuchang deposit. 1—Quaternary alluvium deposits; 2—Tamulangou formation of upper Jurassic; 3—Early Yanshanian granite porphyry; 4—Middle Variscan porphyry biotite monzogranite; 5—Strata occurrence(tuff in late Jurassic); 6—Measured normal fault and its dip angle; 7—Concealed fault; 8—Ore body and its number; 9—Prospecting line and its number; 10—Sampling location and its number; S1—13QYK1 and samples for S and Pb isotopes; S2—13QYK2 and samples for S and Pb isotopes; S3—14QY; S4—13QY6; S5—13QY25 and the sample for U-Pb Dating; S6—13QY16; S7—13QY11; S8—13QYK3 and samples for S and Pb isotopes; S9—13QY2-1; S10—13QY2-2; S11—13QY3; S12—13QY13.

In 2005, the Tenth Institute of Geology and Mineral Exploration and Development of Inner Mongolia discovered a medium-size lead–zinc deposit in Qiyimuchang. This study conducted detailed field geological surveying, petrographic and mineralogical observation, trace element analysis of volcanic rocks and ores in host rocks, and S–Pb isotopic analysis of ores to trace the source of ore-forming materials. Furthermore, the zircon U–Pb age of volcanic host rocks was determined to limit the diagenetic and metallogenic age.




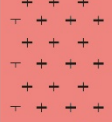
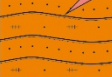

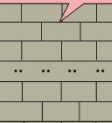
## 2. Geological Background

The Qiyimuchang lead–zinc deposit is located in the east of CAO, in the east of the Xing'an–Mongolia orogenic belt and in the southeast of the Erguna Massif (Figure 1B). The Erguna Massif lies adjacent to the Mongolia–Okhotsk suture zone in the northwest and the Xing'an Massif in the southeast. In the Erguna Massif, along the NE striking Derbugan fault, many lead–zinc, copper–molybdenum, and gold deposits have been found. Most lead–zinc deposits are controlled by secondary faults along regional faults, which directly control the shape and distribution of ore bodies [1–4]. Among them, faults striking NE, NNE, NW are mostly ore guiding and hosting structures of lead–zinc deposits. These lead–zinc deposits primarily occur in middle-upper Jurassic and lower Cretaceous volcanic rocks. The ore bodies are mostly vein-shaped, stockwork-shaped, and lenticular, mainly hypabyssal or ultra-hypabyssal [5–7]. The ore-forming fluid is characterized by medium low temperature and medium-low salinity. The ore body, which belongs to the epigenetic filling vein lead–zinc deposit, generally formed after the formation of the surrounding rocks (andesite, rhyolite, tuff, etc.) [17,18]. Therefore, the vein lead–zinc deposits in this area have similar metallogenic geological conditions. Unlike most lead–zinc deposits located west of the Derbugan fault, the Qiyimuchang lead–zinc deposit lies east of the Derbugan fault (Figure 1B). The Derbugan fault is a strike-slip fault located in the Erguna Massif. It is a large NE striking extensional deformation zone that was very active from the Late Jurassic to early Cretaceous [19].



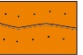
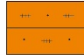


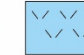



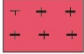

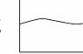

The main exposed strata in the area include the lower Carboniferous Morgenhe Formation ( $C_{1m}$ ), the lower Permian Xinyigenhe Formation ( $P_{1x}$ ), the upper Jurassic Tamulangou Formation ( $J_{3tm}$ ), the Marketouebo Formation ( $J_{3mk}$ ), and Quaternary alluvium deposits (Q). The common rock combinations of each formation are presented in Figure 2.  $J_{3tm}$  and Q are exposed in the Erguna area (Figure 1C). With an overall strike of NE, a dip of NW, and a dip angle of 20–50°,  $J_{3tm}$  is mainly composed of basaltic andesite, andesite, andesitic crystal debris tuff, tuffaceous sandy conglomerate, and tuff. In particular, the lead–zinc orebodies mainly occur in the andesitic crystal debris tuff.

Two stages of plutonism masses (Variscan and Yanshanian) are exposed in the south of the Erguna area (Figure 1C). The lithology of Variscan granite is light flesh red porphyritic biotite monzogranite with medium-fine grained texture (composed of quartz, orthoclase, plagioclase, and biotite). The lithology of Yanshanian granite is light flesh red syenite granite porphyry with porphyritic texture. The matrix is mainly composed of orthoclase, albite, quartz, and biotite. This pluton is in contact with the NE fault of the Tamulangou Formation and intruded into the Variscan rock mass (Figure 1C). No lead–zinc ore body has been found in the intrusive body of the mining area.

The mining area includes NW striking and 60–70° SW dipping faults. These faults comprise the ore bearing structure of the lead–zinc orebodies. NE and near SN normal faults are developed in the mining area (Figure 1C). The NE striking fault in the mining area extends over 4 km, towards NW and dipping approximately 70°. The strike and dip are close to those (tuff, andesite, rhyolite, etc.) of the Tamulangou Formation. In the south of the mining area, the NE striking fault serves as the boundary between the Tamulangou Formation and granite porphyry, whereas in the north, it cuts through the Tamulangou Formation and the lead–zinc ore body, clearly indicating post metallogenic faulting.

Formation or intrusive rock	Code	Column	Spatial relationship with rock below	Common rock types
Quaternary alluvium deposits	Q		unconformity covered	Alluvionar deposits
Manketouebo Formation	J <sub>3</sub> mk		unconformity covered	Rhyolitic tuff and Rhyolite
Tamulangou Formation	J <sub>3</sub> tm		fault	Andesitic tuff and Andesite
Yanshanian granite	γπ <sub>5</sub> <sup>2</sup>		intrusive	Light flesh red syenite granite porphy
Xinyigenhe Formation	P <sub>1</sub> x		unconformity covered	Greywacke and Slate
Variscan granite	ηγ <sub>4</sub> <sup>2(2)</sup>		intrusive	Light flesh red porphyritic biotite monzogranite
Morgenhe Formation	C <sub>1</sub> m			Limestone and Siltstone

	1		2		3		4		5		6		7
	8		9		10		11		12		13		14

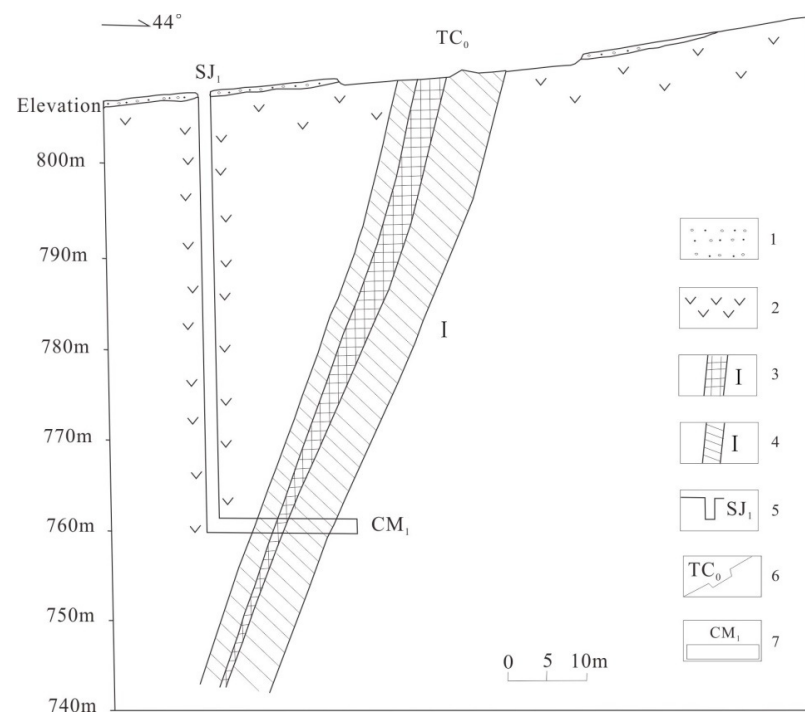
**Figure 2.** Common rock combinations of each formation around the Qiyimuchang deposit. 1—Limestone; 2—Siltstone; 3—Slate; 4—Greywacke; 5—Andesite; 6—Andesitic tuff; 7—Rhyolite; 8—Rhyolitic tuff; 9—Alluvium deposits; 10—Variscan light flesh red porphyritic biotite monzogranite; 11—Yanshanian light flesh red syenite granite porphyry; 12—Intrusive; 13—Unconformity covered; 14—Fault.

### 3. Deposit Geology

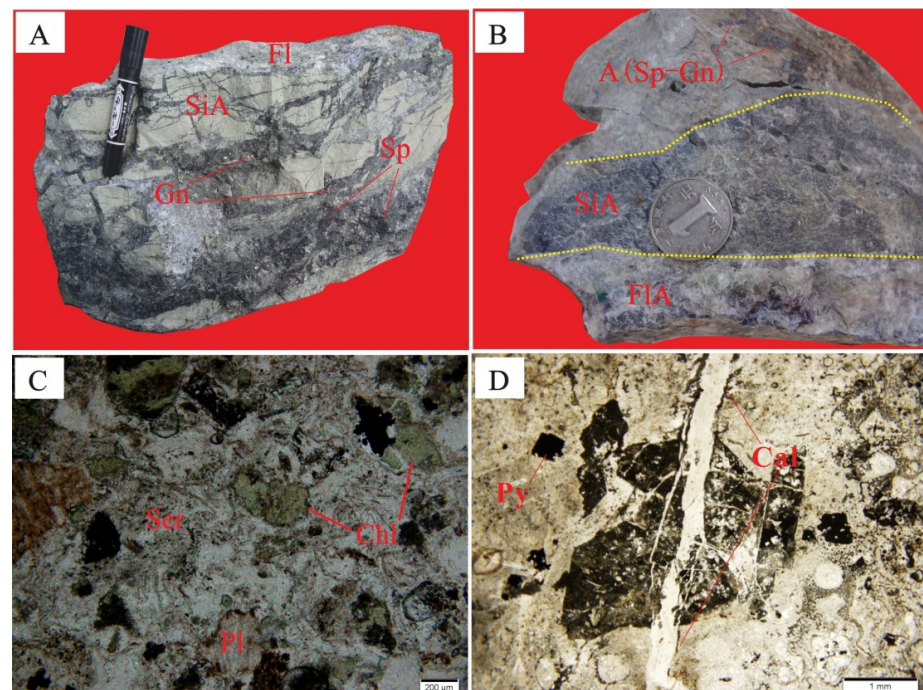
The exploration project from the Tenth Institute of Geology and Mineral Exploration and Development of Inner Mongolia delineated three lead–zinc industrial orebodies in the mining area (Figure 1C). The orebodies occur as veins (Figures 1C and 3) in the NW fracture in the Tamulangou Formation. The ore-hosting rocks are andesite, andesitic tuff, and rhyolite. The orebody trends NW (296–338°), inclining SW (Figure 3), and the dip angle varies from 62° to 77°. The exposed length of the ore body on the surface is tens to hundreds of meters, the thickness is 1–7 m, and the average ore grade is Pb 3.1% and Zn 4.5%.

Quartz and fluorite are gangue minerals of the ore also developed in the altered andesite wall rock (Figure 4A,B). Further characteristic alteration minerals are sericite, chlorite, and epidote (Figure 4C). Gangue minerals are mainly carbonates in the late metallogenic period (Figure 4D). Among them, silicification, fluoritization, and pyritization are most closely related to mineralization.



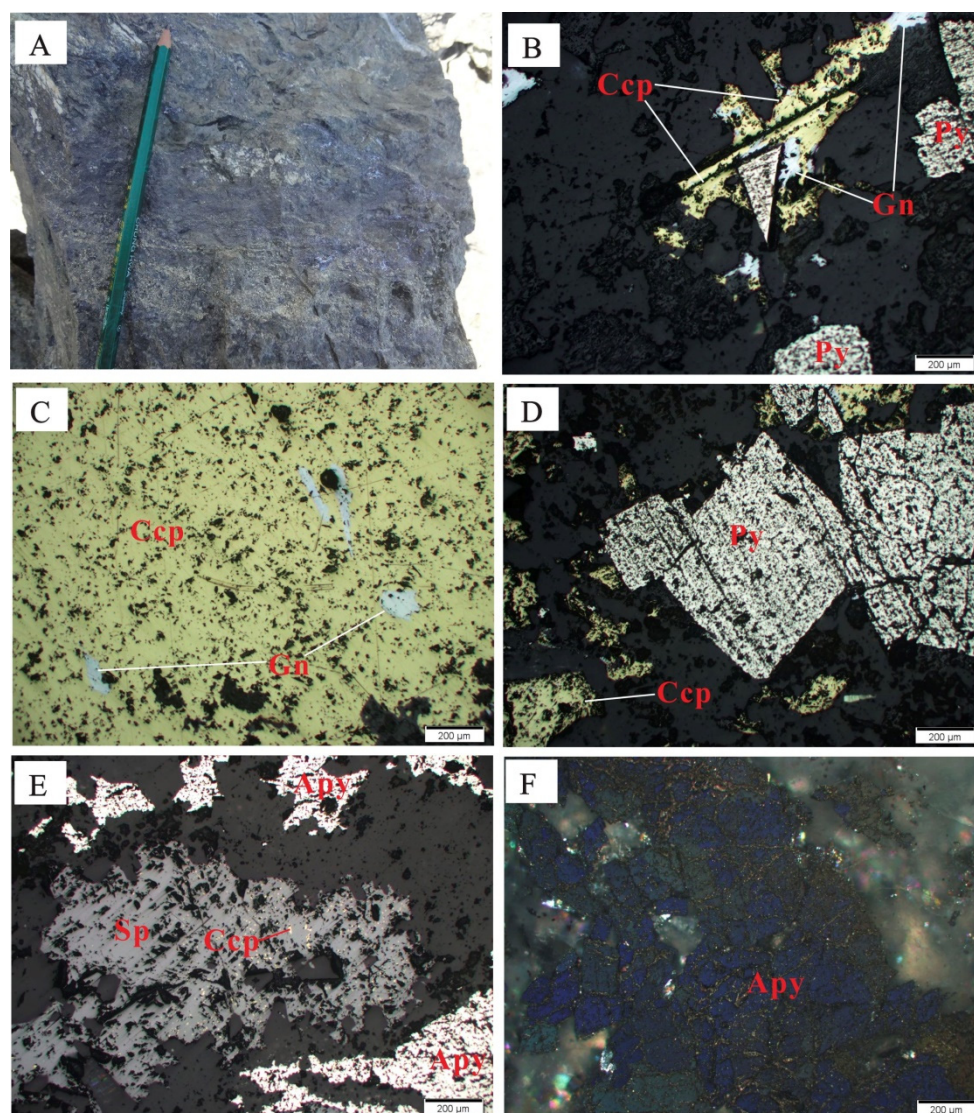


**Figure 3.** Cross-section of I orebody in No.0 exploration line [16]. 1—Quaternary alluvium deposits; 2—Andesite; 3—Orebody; 4—Alteration zone; 5—SJ<sub>1</sub>:shaft and its number; 6—TC<sub>0</sub>: exploratory trench; 7—CM<sub>1</sub>: footwall. Hydrothermal alteration is common in the surrounding andesites of the upper and lower walls of the ore body forming an alteration zone with a width of 1–5 m.



**Figure 4.** Alteration characteristics and micrographs of andesite and andesitic crystalline tuff of the Qiyimuchang lead zinc deposit. (A)—Andesite (host rock) penetrated by veins; (B)—Silicification and fluoritization alteration; (C)—Chloritization in andesitic crystalline tuff (single-polarized transmitted light); (D)—Later stage of carbonation, with visible carbonate veins cutting through amphibole (single polarized transmitted light); Py—pyrite; Gn—galena; Sp—sphalerite; Pl—plagioclase; Chl—chlorite; SiA—silicified andesite, Fl—fluorite, FlA—fluoritized andesite, A(Sp—Gn)—lead and zinc sulfide, Ser—sericite, Cal—carbonate.

Metal sulfide minerals in the ore mainly consist of sphalerite, galena, chalcopyrite, and pyrite, and gangue include quartz, fluorite, and calcite. Ore minerals in the ore show vein like, fine vein like, and mesh vein like structures (Figures 4A and 5A) and disseminated structures. The minerals in the ore show metasomatic dissolution structure (Figure 5B), metasomatic residual structure (Figure 5C), pseudocrystalline structure (Figure 5D), solid solution separation structure (Figure 5E), and crushing structure (Figure 5F). According to the alternation of minerals in the ore and the alteration characteristics of surrounding rocks, hydrothermal mineralization occurred through three stages, pyrite arsenopyrite (mainly quartz, arsenopyrite and a small amount of pyrite), sphalerite chalcopyrite (pyrite, chalcopyrite, sphalerite, galena, fluorite, and a small amount of tetrahedrite), and quartz calcite (quartz calcite veinlets with a small amount of pyrite).



**Figure 5.** Ore samples and micrographs of the Qiyimuchang deposit. (A)—Massive ore; (B)—Galena irregularly distributed on the edge of pyrite, metasomatizing and dissolving pyrite(single polarized reflected light); (C)—Galena remaining as an island in chalcopyrite and is metasomatized by chalcopyrite to form a residual structure(single polarized reflected light); (D)—Pyrite presenting pseudocrystalline structure of arsenopyrite after replacing arsenopyrite(single polarized reflected light); (E)—Emulsion droplets of chalcopyrite in the matrix of sphalerite that show an exsolution structure (single polarized reflected light); (F)—Arsenopyrite in a crushed structure(orthogonally polarized reflected light).



## 4. Samples and Methods

### 4.1. Rare Earth and Trace Elements

In order to explore the relationship between host rock and mineralization of the Qiyimuchang lead–zinc deposit, samples were collected from No. 2 and No. 3 ore bodies and their contact zones for the study of ore, altered mineralized volcanic rocks, rare earth elements (REEs), and trace elements of unaltered volcanic rocks. The sample fragmentation and testing processes were completed at the Key Laboratory of Mineral Resources Evaluation in Northeast Asia of Jilin University. Samples for trace elements and REEs were melted in a Teflon melting tank. The samples is pretreated by the electrothermal plate digestion and dilution method, which dissolved by  $\text{HNO}_3$ ,  $\text{HF}$ , and  $\text{HClO}_4$ , and diluted to 10 mL with 3%  $\text{HNO}_3$  after constant volume with ultrapure water. Shake well and then measured by double focusing high-resolution plasma mass spectrometer ICP-MS (Finnigan MAT Company, Germany). Details of the specific sample processing are available in relevant literature [20,21].

### 4.2. S and Pb Isotope

In order to explore the material source of the Qiyimuchang lead–zinc deposit, samples of S and Pb isotopes of pyrite and sphalerite in the main metallogenic stage were all collected from the vein ores of No. 2 and No. 3 ore bodies. The selection of single mineral samples was completed at the Hebei Langfang Yuneng Rock and Mineral Sorting Technology Service Co., Ltd., and sample testing was completed at the Analysis and Testing Research Center of Beijing Institute of Geology of Nuclear Industry. Sulfide single mineral and cuprous oxide were ground and mixed evenly according to a certain proportion, heated under vacuum up to  $2.0 \times 10^{-2}$  Pa, and the reaction temperature was 980 °C. Oxidation reaction was allowed to take place in order to produce sulfur dioxide gas, which was collected using the freezing method, and the sulfur isotope composition was analyzed using the MAT 251 gas isotope mass spectrometer (Finnigan MAT Company, Germany). According to test results based on the  $\delta^{34}\text{S}_{\text{V-CDT}}$ , the accuracy was  $\pm 0.2\%$ . The Pb isotope sample was first decomposed by mixing with acid, and lead was then separated using the resin exchange method. After steaming dry, the lead isotope was measured using the IsoProbe-T hot surface ionization mass spectrometer (MicroMass Company, Britain), and the analysis accuracy is better than 0.005%. Details of the specific experimental test process are available in relevant literature [22].

### 4.3. Zircon U-Pb Dating

In order to define the diagenetic and metallogenic age of the Qiyimuchang lead–zinc deposit, andesitic tuff (13QY25) of the host rock was collected from the shaft of No. 2 ore body, and zircon U-Pb dating was carried out. Andesitic tuff is characterized by mottled structure and crystalline lithic tuff structure. The rock is mainly composed of lithoclasts and crystalloclasts and cemented by volcanic ash. Among them, rock debris (mainly composed of andesite) and crystalline debris (mainly plagioclase and a small amount of quartz and potassium feldspar) are angular, with particle size ranging from 0.5 to 1 mm and a content of approximately 40%. The sorting, target making, CL, and transmission and reflection light photography of zircon were completed at the Hebei Langfang Yuneng Rock and Mineral Sorting Technology Service Co., Ltd., and the testing of zircon was completed at the State Key Laboratory of Continental Dynamics of Northwest University. For detailed experimental test flow and data processing methods, please refer to relevant literature [21,23].

## 5. Results

### 5.1. Characteristics of Trace and Rare Earth Elements

The trace element test results of the ore, volcanic rocks, and altered mineralized volcanic rocks in the mining area are shown in Table 1. The trace elements in the surrounding rocks (kinds are expressed in Table 1) and ore of Qiyimuchang deposit show a relatively

consistent similarity. The content of trace elements in the surrounding rocks was higher than that of the ore, and the contents of large-ion lithophile elements (Rb, Th, U) were also relatively high (up to  $111.00 \times 10^{-6}$ – $260.00 \times 10^{-6}$ ,  $6.46 \times 10^{-6}$ – $15.25 \times 10^{-6}$ ,  $1.58 \times 10^{-6}$ – $4.57 \times 10^{-6}$ ). Among high-field-strength elements (HFSEs), Zr showed the highest content, reaching up to  $233.00 \times 10^{-6}$ – $420.00 \times 10^{-6}$ , followed by Nb ( $10.60 \times 10^{-6}$ – $17.8 \times 10^{-6}$ ) and Y ( $18.70 \times 10^{-6}$ – $44.50 \times 10^{-6}$ ), Ta showed relatively low content ( $0.70 \times 10^{-6}$ – $1.20 \times 10^{-6}$ ). As shown in Figure 6A, the volcanic rocks and ores of the Qiyimuchang lead–zinc deposit show relative enrichment of Th, U, and other large-ion lithophile elements (LILEs), while some HFSEs such as Ta, Nb, and Y show a trend of relative loss, reflecting the characteristics of intraplate volcanic rocks to a certain extent [24]. The relative contents of Nb and Ta elements showed weak negative anomalies, Ba, Sr, and other LILEs showed clear losses, and some LILEs such as Rb showed relatively high contents. The characteristics of these elements may indicate that crustal materials participated in the magmatic process. The distinct negative anomalies of Sr may be attributable to the residue of plagioclase and other source areas in the rock and strong alteration of the rock.

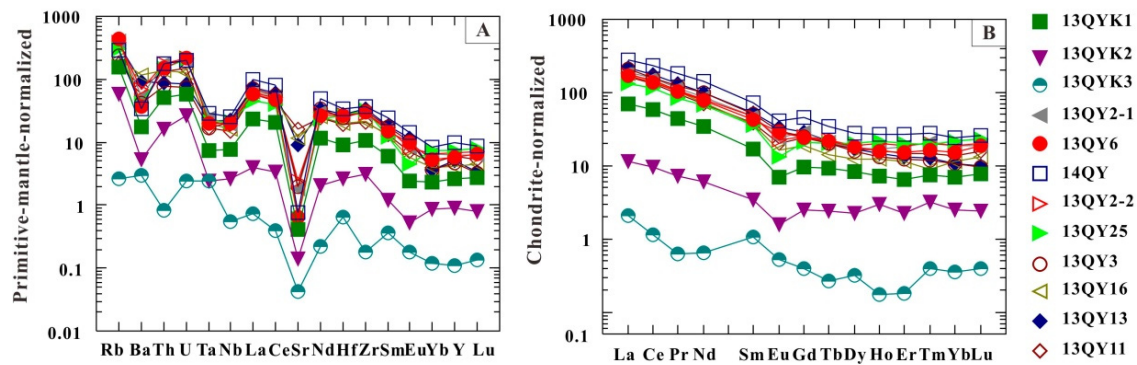
**Table 1.** Trace element (mg/kg) content of the representative rocks and ores in the Qiyimuchang deposit.

	13QYK1	13QYK2	13QYK3	13QY2-1	13QY6	14QY	13QY2-2	13QY25	13QY3	13QY16	13QY13	13QY11
Sample Description	Vein Ore	Massive Ore	Massive Ore	Mineralized Rhyolite	Mineralized Tuff	Altered Andesite	Rhyolite	Andesitic tuff	Basaltic Andesite	Rhyolitic Tuff	Andesite	Dacitic Crystal Tuff
Rb	100.00	36.80	1.70	260.00	276.00	182.50	246.00	192.00	149.00	131.50	229.00	111.00
Sr	8.70	3.00	0.90	39.00	13.90	16.00	50.80	13.30	41.70	250.00	190.00	338.00
Ba	122.50	36.80	20.40	368.00	261.00	235.00	482.00	293.00	286.00	825.00	629.00	516.00
Ga	12.00	6.50	3.00	19.40	19.50	22.80	20.20	22.20	23.70	18.10	23.50	18.30
Nb	5.50	1.90	0.40	13.30	13.90	17.80	13.60	15.50	14.70	11.70	15.90	10.60
Ta	0.30	0.10	0.10	1.00	0.80	1.20	0.90	0.90	0.70	0.80	0.90	0.70
Zr	122.00	35.00	2.00	319.00	333.00	420.00	324.00	359.00	355.00	245.00	380.00	233.00
Hf	2.80	0.80	0.20	8.30	8.10	10.40	8.40	8.20	7.50	6.10	8.50	6.00
Th	4.43	1.40	0.07	14.95	12.50	15.25	15.20	12.80	6.46	11.80	7.46	11.35
U	1.22	0.56	0.05	4.14	4.57	4.23	4.48	4.40	1.58	2.71	1.76	3.13
V	14.00	9.00	5.00	19.00	30.00	20.00	18.00	15.00	135.00	35.00	147.00	50.00
Cr	9.00	10.00	20.00	10.00	10.00	10.00	8.00	10.00	50.00	20.00	50.00	40.00
Sn	17.00	13.00	1.00	5.00	5.00	5.00	5.00	9.00	3.00	2.00	3.00	2.00
Cs	7.26	3.02	0.24	16.30	17.35	16.25	13.65	10.50	8.31	42.00	14.75	14.75
Y	12.00	4.10	0.50	28.10	26.10	44.50	30.80	32.90	21.60	18.70	23.20	26.80
W	5.00	4.00	3.00	2.00	16.00	2.00	2.00	19.00	9.00	2.00	7.00	2.00
La	16.40	2.70	0.50	44.30	39.80	66.70	42.10	31.00	49.20	43.10	51.80	39.40
Ce	36.20	5.90	0.70	94.90	84.60	142.50	90.80	69.90	98.20	87.90	107.50	79.50
Pr	4.17	0.69	0.06	10.70	9.83	17.05	10.30	8.01	11.80	9.72	12.50	8.99
Nd	15.80	2.80	0.30	40.00	36.20	66.00	38.20	31.50	45.70	34.00	46.80	32.50
Sm	2.62	0.53	0.16	7.13	6.49	10.90	7.33	5.36	7.74	5.70	8.00	5.75
Eu	0.40	0.09	0.03	1.38	1.66	2.38	1.32	0.76	1.72	0.95	1.92	1.19
Gd	1.99	0.52	0.08	5.86	4.95	9.40	5.19	4.34	5.16	3.91	6.01	4.87
Tb	0.35	0.09	0.01	0.79	0.81	1.29	0.85	0.76	0.76	0.53	0.82	0.75
Dy	2.11	0.57	0.08	4.51	4.53	7.17	4.81	5.17	4.02	3.14	4.24	4.34
Ho	0.41	0.17	0.01	0.96	0.89	1.53	1.16	1.21	0.75	0.70	0.84	0.92
Er	1.08	0.37	0.03	2.96	2.52	4.40	3.15	3.38	2.03	1.88	2.16	2.46
Tm	0.19	0.08	0.01	0.53	0.42	0.70	0.52	0.49	0.30	0.23	0.32	0.37
Yb	1.17	0.43	0.06	3.24	2.60	4.08	3.24	3.71	1.81	1.94	1.80	2.30
Lu	0.20	0.06	0.01	0.47	0.48	0.65	0.52	0.59	0.24	0.33	0.25	0.40
ΣREE	83.09	15.00	2.04	217.73	195.78	334.75	209.49	166.18	229.43	194.03	244.96	183.74
ΣLREE	75.59	12.71	1.75	198.41	178.58	305.53	190.05	146.53	214.36	181.37	228.52	167.33
ΣHREE	7.50	2.29	0.29	19.32	17.20	29.22	19.44	19.65	15.07	12.66	16.44	16.41
LREE/HREE	10.08	5.55	6.03	10.27	10.38	10.46	9.78	7.46	14.22	14.33	13.90	10.20
La/Yb	9.45	4.23	5.61	9.22	10.32	11.02	8.76	5.63	18.33	14.98	19.40	11.55
Eu/Eu*	0.45	0.46	0.62	0.56	0.75	0.62	0.54	0.41	0.68	0.51	0.71	0.59
δCe	1.03	1.02	0.82	1.02	1.00	0.99	1.02	1.04	0.95	0.99	0.99	0.98

As shown in Table 1, clear differences could be observed in the total amount of REEs, light rare earth elements (LREEs), and heavy rare earth elements (HREEs) in ores and volcanic rocks in the Qiyimuchang mining area. In the volcanic rocks, the total amounts of REEs, LREEs, and HREEs were high, reaching up to  $166.18 \times 10^{-6}$ – $334.75 \times 10^{-6}$ ,  $167.33 \times 10^{-6}$ – $305.53 \times 10^{-6}$ , and  $12.66 \times 10^{-6}$ – $29.22 \times 10^{-6}$ , respectively. In contrast, the total amounts of REEs, LREEs, and HREEs were lower in the ore at  $2.04 \times 10^{-6}$ – $83.09 \times 10^{-6}$ ,  $1.75 \times 10^{-6}$ – $75.59 \times 10^{-6}$ , and  $0.29 \times 10^{-6}$ – $7.5 \times 10^{-6}$ , respectively, indicating that a large number of REEs were released with the ore-forming materials during mineralization, and the exchange of REEs occurred in the hydrothermal system. The LREE/HREE ratio and La/Yb ratio of all samples tested were greater than one, indicating a right dipping distribution mode. Moreover, the rare earth distribution modes of volcanic rocks and ores were very similar (Figure 6B), indicating that they may belong to the same source area and are the products of different stages of homologous magma activities. The Ce/Yb ratio of all samples ranged from 11.60 to 59.70, and the Th/Yb ratio ranged from 1.20 to 6.20, indicating that differential crystallization occurred in the



process of magmatic evolution [26]. According to the trend of rare earth composition curve  $\text{Eu}/\text{Eu}^*$  value, all samples showed weak negative Eu anomaly, with the  $\text{Eu}/\text{Eu}^*$  value ranging from  $0.41 \times 10^{-6}$  to  $0.76 \times 10^{-6}$  ( $0.58 \times 10^{-6}$  on average). The relative loss of HREEs indicates the presence of residual garnet in the magma source area. The negative Eu anomaly may indicate the separation of feldspar and other minerals from felsic magma during the differential crystallization of magma. It can also be said that feldspar remained in the source area during the partial melting [27].



**Figure 6.** Primitive-mantle-normalized trace element diagrams (A) (normalized with data from [25]) and chondrite-normalized REE patterns (B) normalized with data from [25] for the representative rocks (kinds are expressed in Table 1) and ores in the Qiyimuchang deposit.

### 5.2. Characteristics of S and Pb Isotopic

As shown in Table 2 and Figure 7, the Qiyimuchang mining area is similar to other lead–zinc deposits in the same area. The sulfur isotopes are distributed in a tower-like manner,  $\delta^{34}\text{S}$  values are positive, and the change of  $\delta^{34}\text{S}$  value in a certain range is small, which indicates that the sulfur isotopic composition is relatively stable. The variation range was from +1.60‰ to +4.80‰, the average value was +4.00‰, the range was  $R = 3.20$ , and the standard deviation was  $S = 1.10$ . Among them, the pyrite  $\delta^{34}\text{S}$  value was between +1.60‰ and +4.30‰, which is slightly less than that of the sphalerite  $\delta^{34}\text{S}$  value (+3.80‰–+4.80‰). The reason for this phenomenon may be that the sulfur fractionation did not reach equilibrium during the evolution of the hydrothermal system; it may also be due to the loss of  $^{34}\text{S}$  in the ore-forming fluid caused by the high oxygen fugacity in the evolution of the hydrothermal fluid [28,29].

**Table 2.** Sulfur isotope data of ore minerals from typical lead–zinc deposits in Erguna metallogenic belt.

Deposit	Sample	Result	Source
		$\delta^{34}\text{S}_{\text{V-CDT}}$ (‰)	
Qiyimuchang	sphalerite(13QYK1)	4.80	this paper
	pyrite (13QYK1)	4.30	
	sphalerite (13QY6)	4.70	
	sphalerite (13QYK2)	4.40	
	pyrite (13QYK2)	4.30	
	sphalerite (13QYK3)	3.80	
	pyrite (13QYK3)	1.60	

Table 2. Cont.

Deposit	Sample	Result	Source
		$\delta^{34}\text{S}_{\text{V-CDT}} (\text{‰})$	
Jiawula	galena	3.90	[30]
	galena	4.10	
	pyrite	3.70	
	pyrite	3.20	
	pyrite	2.80	
	sphalerite	3.90	
	sphalerite	3.80	
Dongjun	galena	4.48	[31]
	pyrite	6.76	
	pyrite	6.63	
	pyrite	6.97	
	pyrite	6.89	
Derbur	pyrite	5.20	[3]
	pyrite	5.40	
	pyrite	4.90	
	pyrite	5.20	
	sphalerite	5.00	
	sphalerite	5.20	
	galena	2.90	
	galena	3.60	

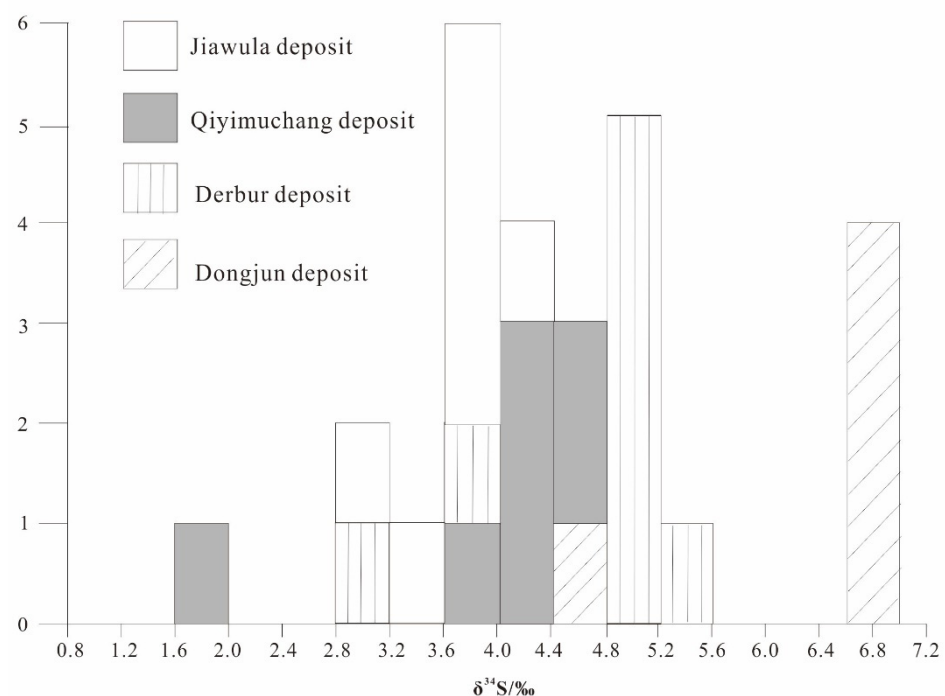


Figure 7. Sulfur isotope abundances of sulfide in typical lead zinc deposits in Erguna metallogenic belt.

The test results were consistent with those of the sulfur isotope analysis. The lead isotopic compositions of seven pyrite and sphalerite samples and other deposits in the same area are listed in Table 3. The analysis results show that the changes of  $^{208}\text{Pb}/^{204}\text{Pb}$ ,  $^{207}\text{Pb}/^{204}\text{Pb}$ , and  $^{206}\text{Pb}/^{204}\text{Pb}$  are relatively stable at 38.15–38.39, 15.55–15.62, and 18.33–18.41, respectively. The distribution range is relatively concentrated and the change is small, indicating that the lead in the sulfide of the Qiyimuchang deposit has the characteristics of normal lead [32].

**Table 3.** Lead isotope data of ore minerals from typical lead–zinc deposits in Erguna metallogenic belt.

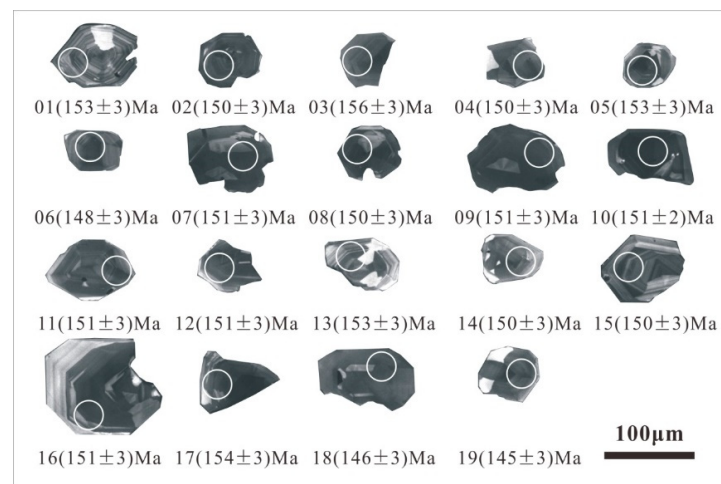
Deposit	Sample	Isotope Ratio			$\mu$	$\omega$	$\Delta\beta$	$\Delta\gamma$	Source
		$^{208}\text{Pb}/^{204}\text{Pb}$	$^{207}\text{Pb}/^{204}\text{Pb}$	$^{206}\text{Pb}/^{204}\text{Pb}$					
Qiyimuchang	Sphalerite (13QYK1)	38.26	15.58	18.35	9.44	35.92	16.83	27.05	This paper
	Pyrite (13QYK1)	38.15	15.55	18.33	9.37	35.31	14.61	24.15	
	Sphalerite (13QY6)	38.29	15.59	18.36	9.45	36.08	17.35	27.86	
	Sphalerite (13QYK2)	38.21	15.57	18.34	9.41	35.66	15.85	25.82	
	Pyrite (13QYK2)	38.29	15.59	18.36	9.45	36.09	17.41	27.94	
	Sphalerite (13QYK3)	38.38	15.62	18.38	9.50	36.58	19.17	30.27	
	Pyrite (13QYK3)	38.39	15.62	18.41	9.50	36.51	19.31	30.65	
Erdaohezi	Sphalerite	38.24	15.56	18.44					[10]
	Sphalerite	38.26	15.57	18.44					
	Sphalerite	38.22	15.56	18.44					
	Pyrite	38.19	15.55	18.13					
	Sphalerite	38.23	15.56	18.44					
	Pyrite	38.20	15.55	18.43					
	Sphalerite	38.25	15.57	18.44					
Dongjun	Pyrite	38.10	15.53	18.34					[31]
	Pyrite	38.42	15.63	18.43					
	Pyrite	38.26	15.58	18.38					
	Pyrite	38.13	15.54	18.35					
	Pyrite	38.15	15.55	18.35					
	Galena	37.98	15.49	18.32					
	Galena	38.01	15.52	18.33					
	Galena	38.20	15.56	18.37					
	Sphalerite	38.16	15.55	18.36					
Jiawula	Sphalerite	38.17	15.55	18.36					[30]
	Galena	38.15	15.55	18.33					
	Pyrite	38.08	15.54	18.28					
	Galena	38.14	15.55	18.33					
	Sphalerite	38.14	15.54	18.33					
	Pyrite	38.12	15.54	18.31					
	Pyrite	38.14	15.55	18.33					
	Sphalerite	38.14	15.55	18.34					
	Upper crust						>18	>45	
	Mixing of crust and mantle						12–40	20–45	
	Mantle						–5–15	–5–20	

Note: isotope parameters are calculated by using geokit software developed by Lu [33]; Upper crust, crust mantle mixing and mantle lead isotope parameters are cited from Li and Zhao [34].  $\mu = ^{238}\text{U}/^{204}\text{Pb}$ ;  $\omega = ^{232}\text{Th}/^{204}\text{Pb}$ ;  $\Delta\beta = [\beta/\beta\text{M}(t)-1] \times 1000$ ;  $\Delta\gamma = [\gamma/\gamma\text{M}(t)-1] \times 1000$ .  $\beta$  and  $\gamma$  are current mantle values.  $\beta\text{M}(t)$  and  $\gamma\text{M}(t)$  are mantle values at “t”. The “t” value is referred from the age of the Jiawula lead zinc deposit as 142 Ma.

### 5.3. Zircon U-Pb Ages in Andesitic Tuff

Zircons in andesitic crystal debris tuff in the Qiyimuchang mining area exhibit high transparency, medium crystal form integrity, aggregation, and octahedral shape, and the particle size is generally between 73 and 154  $\mu\text{m}$ , with high automorphism and clear oscillatory ring (Figure 8). The Th and U contents of zircon were 128.00–1704.31 mg/kg and 138.07–1079.35 mg/kg, respectively, and the Th/U ratio was 0.41–2.17. All values being greater than 0.40 (Table 4) suggests that the zircons measured are of typical magmatic origin [35,36].



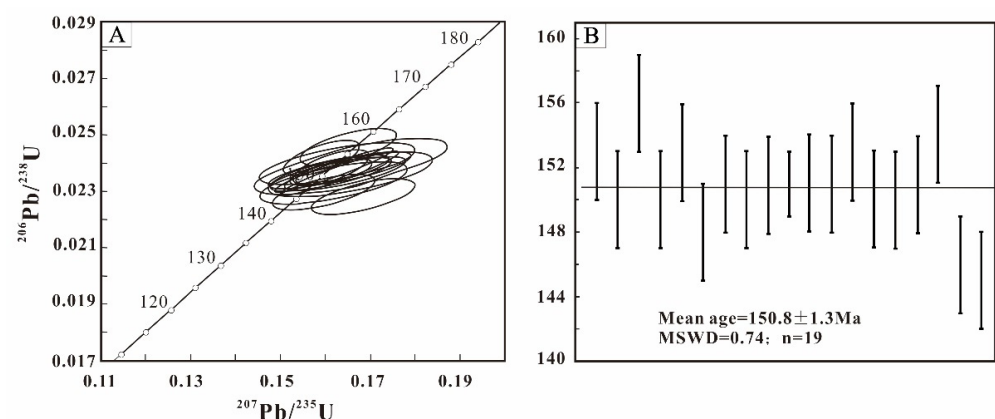


**Figure 8.** Zircon CL image of andesitic clastic lithic tuff in the host rock of the Qiyimuchang lead–zinc deposit.

**Table 4.** LA-ICP-MS zircon U–Th–Pb dating results of the andesite tuff from Qiyimuchang deposit.

Number	U (mg/kg)	Th (mg/kg)	Th/U	Isotope Ratio				Age (Ma)							
				$^{207}\text{Pb}/^{206}\text{Pb}$	$1\sigma$	$^{207}\text{Pb}/^{235}\text{U}$	$1\sigma$	$^{206}\text{Pb}/^{238}\text{U}$	$1\sigma$	$^{206}\text{Pb}/^{238}\text{U}$	$1\sigma$	$^{207}\text{Pb}/^{235}\text{U}$	$1\sigma$	$^{207}\text{Pb}/^{206}\text{Pb}$	$1\sigma$
1	138.07	127.95	0.93	0.05	0.004	0.16	0.012	0.02	0.0005	153	3	153	10	157	119
2	212.64	301.13	1.42	0.05	0.004	0.17	0.012	0.02	0.0005	150	3	156	11	236	127
3	407.5	186.43	0.46	0.05	0.002	0.16	0.007	0.02	0.0004	156	3	155	6	135	68
4	314.49	541.42	1.72	0.05	0.003	0.16	0.008	0.02	0.0004	150	3	152	7	180	87
5	266.67	579.66	2.17	0.05	0.003	0.16	0.010	0.02	0.0005	153	3	154	9	168	100
6	378.43	691.25	1.83	0.05	0.004	0.16	0.011	0.02	0.0005	148	3	152	9	213	115
7	650.57	404.52	0.62	0.05	0.002	0.16	0.007	0.02	0.0004	151	3	154	6	210	67
8	379.26	236.84	0.62	0.05	0.003	0.16	0.008	0.02	0.0004	150	3	153	7	197	79
9	322.72	132.19	0.41	0.05	0.003	0.16	0.008	0.02	0.0004	151	3	154	7	201	80
10	1079.35	1704.31	1.58	0.05	0.001	0.16	0.004	0.02	0.0004	151	2	153	4	186	30
11	239.23	354.09	1.48	0.05	0.003	0.16	0.009	0.02	0.0004	151	3	150	7	136	87
12	292.55	464.93	1.59	0.05	0.002	0.16	0.008	0.02	0.0004	151	3	152	7	172	74
13	370.54	636.61	1.72	0.05	0.004	0.17	0.012	0.02	0.0005	153	3	158	11	237	123
14	285.85	488.21	1.71	0.05	0.003	0.16	0.010	0.02	0.0005	150	3	153	9	193	102
15	450.38	303.83	0.67	0.05	0.003	0.17	0.008	0.02	0.0004	150	3	156	7	239	80
16	346.85	203.08	0.59	0.05	0.004	0.16	0.012	0.02	0.0005	151	3	153	10	183	126
17	528.17	329.13	0.62	0.05	0.002	0.16	0.006	0.02	0.0004	154	3	150	5	87	51
18	551.19	329.26	0.60	0.05	0.003	0.16	0.008	0.02	0.0004	146	3	150	7	213	75
19	305.45	477.73	1.56	0.05	0.003	0.17	0.008	0.02	0.0004	145	3	158	7	351	70

The  $^{206}\text{Pb}/^{238}\text{U}$  surface ages of 19 measuring points ranged between  $(145 \pm 3)$  Ma and  $(156 \pm 3)$  Ma. On the zircon U–Pb age harmony diagram (Figure 9), the age data are located on and near the harmony line. The weighted mean age was  $(150.8 \pm 1.3)$  Ma (MSWD = 0.74, Confidence 95%), representing the crystallization age of andesitic tuff, i.e., late Jurassic.



**Figure 9.** Zircon U–Pb concordia diagram (A) and weighted average diagram (B) for the andesitic lithic crystal tuff from the Qiyimuchang deposit.

## 6. Discussion

### 6.1. Source of Ore-Forming Materials

#### 6.1.1. Trace and Rare Earth Element Evidence

The composition of trace elements in rocks and ores has a certain geochemical significance. The study of the geochemical characteristics of ore bodies and surrounding rocks is of great significance to the study of the whole deposit. The host rock of the Qiyimuchang lead–zinc deposit is the volcanic rock of the Tamulangou formation. According to the analysis of the trace characteristic parameters (Table 1) and primitive-mantle-normalized trace element diagrams (Figure 6A) of volcanic rocks and ores in the Qiyimuchang mining area, LILEs, such as Th and U, are relatively enriched in ores and volcanic rocks, while HFSEs, such as Ta and Nb, are relatively depleted and exhibit clear negative Sr anomalies, indicating that a large amount of Sr was lost through serious rock alteration. A distinct negative Nb anomaly could be observed, suggesting that crustal materials might have participated in the magmatic evolution [27]. The distribution pattern of incompatible elements in trace elements showed a relatively similar trend. Th, U, and Rb show clear positive anomalies, the total rake ratio is negative, and Nb and Ta show obvious negative anomalies. These suggest that the tectonic background of volcanic rocks and ores in the Qiyimuchang mining area may correspond to a continental rift environment [37]. The change trends of trace elements in volcanic rocks, mineralized altered volcanic rocks, and ores were relatively similar, but slightly different. The trace elements of the lead–zinc ores appear to not only inherit the characteristics of surrounding rocks, but also retain the characteristics of the metallogenic hydrothermal solution itself.

The content of REEs in volcanic rocks in the Qiyimuchang lead–zinc mining area was higher than that in ore, which may be due to the strong activity of REEs in the process of alteration and mineralization, resulting in the introduction and removal of REEs and metallogenic materials. Nevertheless, the differentiation relationship between REEs has not changed. Therefore, the characteristics of the REE distribution model shown in the diagram still reflect the characteristics of magmatic evolution (Figure 6B). The REE distribution model shows that the ore and volcanic rocks are relatively consistent, indicating that they may originate from homologous areas and the products of different magmatic stages.

In recent years, petrological and geochemical studies of basic volcanic rocks in the Tamulangou Formation in the Erguna Block have shown that the magma source area may be an enriched lithospheric mantle metasomatized by subduction fluid, and that the magma was clearly contaminated by crustal material during magmatic evolution and ascent [38–40]. Therefore, it can be preliminarily ascertained that the metallogenic material and surrounding rock of the Qiyimuchang lead–zinc deposit originate from the same source area and are products of different magmatic stages.

#### 6.1.2. Sulfur and Lead Isotope Evidence

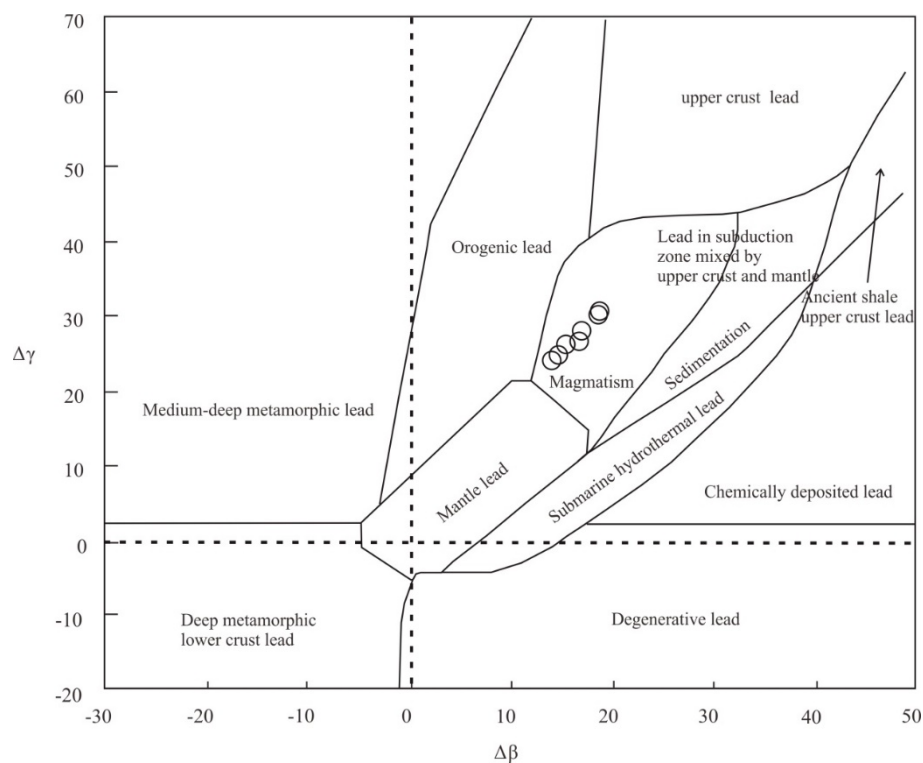
Sulfur is one of the most important metallogenic elements in lead–zinc deposits. The sulfur isotopic composition in the ore can indicate the source and genesis of sulfur in the ore [41]. Therefore, the sulfur stable isotopic composition of metal sulfide in the ore can not only reflect the initial ratio of sulfur stable isotopes, but also reveal the source of ore-forming materials in the deposit in combination with other characteristics [42,43]. Sulfur isotopes are generally believed to have three sources: mantle derived sulfur ( $\delta^{34}\text{S}$  value close to 0, approximately  $0 \pm 3\text{‰}$ ), current seawater sulfur ( $\delta^{34}\text{S}$  value close to  $+20\text{‰}$ ), and reduced sulfur (large negative  $\delta^{34}\text{S}$  values) [44]. The  $\delta^{34}\text{S}$  values of pyrite, sphalerite, and other single minerals in the Qiyimuchang mining area were close to 0, ranging from  $+1.6\text{‰}$  to  $+4.8\text{‰}$ , with an average value of  $+4.0\text{‰}$  and a small fluctuation range, indicating that the source of ore sulfur in the deposit is relatively singular, with the characteristics of deep source sulfur, and the ore-forming materials may be closely related to magmatic intrusion. The  $\delta^{34}\text{S}$  value of pyrite was between  $+1.6\text{‰}$  and  $+4.3\text{‰}$ , which is slightly less than that of sphalerite (from  $+3.8\text{‰}$  to  $+4.8\text{‰}$ ). The reason for this phenomenon may be that sulfur fractionation did not reach equilibrium during the evolution of the hydrothermal system,

reflecting the characteristics of rapid precipitation of ore-forming materials in the process of mineralization [45,46].

In addition, the S isotopic composition of the Qiyimuchang deposit is basically consistent with that of the typical vein lead–zinc deposit in the region (Figure 7), indicating that their genesis may also be consistent.

Lead isotopes can not only be used to determine the metallogenic age of the deposit, but also has very important significance in the study of the source of metallogenic materials [47,48]. Changes in the characteristic values of lead isotopes  $\mu$  can reflect the source of lead. The values of  $\mu$  are 8.92 in the mantle environment, 10.87 in the orogenic belt [49], 8.69–9.24 normally [50], and 9.58 in the upper crust. The  $\mu$  value of ores in the Qiyimuchang lead–zinc deposit was very high at 9.37–9.50 (9.45 on average), falling between the range of the mantle and the upper crust. The variation range of the  $\omega$  value was 35.31–36.58 (36.02 on average), which is higher than that of the mantle (31.84) and lower than that of the crust (36.84) [48]. This suggests that the lead in the Qiyimuchang deposit may be of mixed source comprising the crust and mantle.

In order to eliminate the influence of time factors and better trace the source of ore-forming materials, Zhu et al. [51] proposed the expression of the three isotopes of lead as the relative deviation of the contemporary mantle  $\Delta\alpha$ ,  $\Delta\beta$ ,  $\Delta\gamma$ , and  $\Delta\gamma$ – $\Delta\beta$  genetic classification diagram to trace the source area of lead. In this study, the  $\Delta\beta$  and  $\Delta\gamma$  values of the deposit were calculated using the GeoKit software (Table 3). The  $\Delta\beta$  value of sulfides in the deposit ranged from 14.61 to 19.31, with an average of 17.22, and the  $\Delta\gamma$  value ranged from 2.15 to 30.65, with an average of 27.68. The  $\Delta\beta$  and  $\Delta\gamma$  values of most samples correspond to the crust–mantle mixed source (Table 3), suggesting that the lead in the deposit may originate from a mixed source of the crust and mantle. In the  $\Delta\gamma$ – $\Delta\beta$  genetic classification diagram (Figure 10), all sample data points fall within the lead (magmatism) range of the subduction zone, where the upper crust and mantle are mixed.



**Figure 10.**  $\Delta\gamma$ – $\Delta\beta$  genetic discrimination diagram of lead isotope for the Qiyimuchang lead–zinc deposit (base map from [49]).

Based on the above characteristics of trace elements, REEs, and sulfur and lead isotopes, the metallogenic material source of the deposit can be preliminarily considered to



be a mixed source of the crust and mantle. In the period of tectonic regime transformation, during the early stage of plate subduction, the crust mantle mixture formed by the upwelling of crustal material and mantle material metasomatized by subduction fluid melted again to form magma. Under the background of the extensional structure, magma upwelling occurred along deep faults and transported a certain amount of ore-forming fluid and ore-forming materials to the shallow part. In the process of upward migration, the ore-forming material was contaminated by crust derived material.

### 6.2. Diagenetic and Metallogenic Age

Based on the field geology and underground investigation of the mining area, and according to the cross-cutting and co-association relationship between the lead–zinc ore body and the surrounding rock, the host rock of the Qiyimuchang lead–zinc mining area can be determined to be mainly basaltic andesite and andesitic crystal debris tuff of the Tamulangou Formation. In this study, the zircon LA-ICP-MS U–Pb dating results of andesitic crystal debris tuff reveal that the age of the upwelling, condensation, and crystallization of the diagenetic magma forming the host rock in the area should be  $150.8 \pm 1.3$  Ma, indicating that the lower limit of mineralization of the deposit should be  $150.8 \pm 1.3$  Ma.

Many studies have investigated the metallogenic age of vein lead–zinc silver deposits in the Erguna metallogenic belt. Li, et al. [12] carried out Rb–Sr isotopic dating of sphalerite and pyrite in the Jiawula silver–lead zinc deposit in the south of the Erguna metallogenic belt, and obtained the isochron age of 142 Ma. Li, et al. [52] obtained the sericite  $^{40}\text{Ar}$ – $^{39}\text{Ar}$  plateau age ( $138 \pm 1$  Ma) of the Chaganbulagan lead zinc silver deposit. In recent years, the Rb–Sr isotopic ages have also been obtained for ore minerals in large-vein lead–zinc deposits, such as Billia Valley ( $131.3 \pm 2.4$  Ma), Derbur ( $141 \pm 1.9$  Ma), and Erdaohezi ( $130.5 \pm 3.6$  Ma), which are widely distributed in the northwest of the Derbugan fault in the middle of the Erguna metallogenic belt [5,11,53]. For vein lead–zinc deposits (such as the Dongjun lead–zinc deposit) in the south and east of Derbugan fault, a more accurate Rb–Sr isochron age of sphalerite ( $130.2 \pm 4.4$  Ma) has also been obtained in recent years [54]. On the whole, the metallogenic age of vein lead–zinc silver deposits on the north and south sides of the Derbugan fault in the Erguna metallogenic belt is between 130 and 145 Ma. Therefore, the metallogenic age of the Qiyimuchang lead–zinc deposit should also be this period, i.e., the early Cretaceous. The metallogenic geological background of vein lead–zinc deposits in the Erguna Block is relatively consistent and the metallogenic age is similar, which reflects that the vein lead–zinc silver deposits in this metallogenic belt may be the output of the same metallogenic process.

### 6.3. Metallogenic Dynamic Background

The characteristics of trace elements in the surrounding rock and ore of the Qiyimuchang deposit show that it has the characteristics of intraplate volcanic rocks. Its metallogenic age is the same period as the vein lead–zinc deposit widely developed in the Erguna Block, i.e., the Early Cretaceous (130–140 Ma). According to the study of trace elements in the deposit and the characteristics of regional tectonic evolution, the Erguna block should be under an extensional tectonic background during this period [24,55,56]. A recent study showed that the Erguna Block has been strongly affected by the Mongolian Okhotsk tectonic domain and the Paleo-Pacific tectonic domain since the Mesozoic [57]. Under this background, it becomes unclear whether the large-scale vein lead–zinc mineralization in Erguna Block should be the product of the evolution of the Mongolia Okhotsk tectonic domain or the Paleo-Pacific tectonic domain.

According to the characteristics of volcanic rocks in Northeast China, previous studies believe that the subduction of the Paleo-Pacific Plate began in the early Jurassic [58–61]. During the late Jurassic–Early Cretaceous, the Paleo-Pacific plate was obliquely subducted, resulting in the strike slip nature of the continental margin of Northeast Asia. From the late Early Cretaceous to the Paleogene, the Paleo-Pacific Plate gradually changed from subduction to retreat [62]. Since the late last century, the “scissors” closure of the Mongolian

Okhotsk Ocean from west to east [63–65] has triggered a series of magmatism and copper molybdenum mineralization, which has been widely recognized by scholars [57,66–71]. In recent years, based on the stratigraphic evidence and paleomagnetism evidence, some scholars proposed that the Mongolia Okhotsk Ocean Basin should have been closed in the middle Jurassic. In the late Jurassic, the Erguna Block entered the regional extensional evolution history after the closure of the Mongolia Okhotsk Ocean [62]. The alkaline subalkaline transitional volcanic rock assemblages of the Tamulangou Formation and Manketou'ebo Formation distributed in NE and NNE directions in the Erguna block all reveal the existence of a regional extensional environment [72,73]. At the same time, the vein shaped epithermal lead–zinc deposits distributed in the NNE direction in the block also indicate that the Erguna Block was in an extensional tectonic environment in this period, during which these alkaline subalkaline transitional volcanic rocks and alkaline rhyolites were absent in the east of the Songliao Basin, South Korea, and Japan [70,74]. This further shows that their formation is related to the evolution of the Mongolia Okhotsk tectonic system, but not to the Paleo-Pacific system. Therefore, from late Jurassic to early Cretaceous, the east of the Songliao Basin was mainly controlled by the subduction tectonic system of the Paleo-Pacific Plate, while the Erguna Massif and Xing'an Massif in the west of the Songliao Basin were mainly controlled by the post orogenic extension system of the Mongolia Okhotsk tectonic domain [75]. In conclusion, this paper holds that the large-scale vein lead–zinc mineralization of the Erguna Massif in the early Cretaceous should occur in a post-orogenic extensional tectonic background of the Mongolia Okhotsk tectonic domain.

## 7. Conclusions

1. The Qiyimuchang lead–zinc deposit is similar to the veined lead–zinc–silver deposit widely developed in the region, and their metallogenic ages are relatively consistent, i.e., the early Cretaceous. It is assumed that veined lead–zinc–silver deposits in the metallogenic belt develop according to the same metallogenic process.
2. The large-scale veined lead–zinc mineralization of the Erguna Massif in the early Cretaceous is controlled by the post orogenic extensional tectonic background of the evolution of the Mongolia Okhotsk tectonic domain.
3. The metallogenic material of the Qiyimuchang lead–zinc deposit should have a crust and mantle mixed source. In other words, the metallogenic material is the product of magma formed by the remelting of the crust and mantle mixture derived from the upwelling of the crust material and mantle material metasomatized by the subduction fluid in the early stage, which evolved under the extensional tectonic background.

**Author Contributions:** Conceptualization, M.D. and Y.R.; Investigation, M.D., Y.R., Y.H. and Q.Y.; Methodology, M.D., Q.Y. and Y.H.; Data curation, M.D. and Y.H.; Writing—original draft preparation, M.D.; Writing—review and editing, Y.R., C.X. and T.L.; Supervision and project administration: Y.R. and T.L. All authors have read and agreed to the published version of the manuscript.

**Funding:** This research was funded by the National Key Basic Research and Development Program of China (2013CB429802) and China Geological Survey Project (ZD20220103).

**Data Availability Statement:** The data presented in this study are available on request from the corresponding author.

**Acknowledgments:** The authors would like to thank all the reviewers who participated in the review and MJEditor ([www.mjeditor.com](http://www.mjeditor.com)) for its linguistic assistance during the preparation of this manuscript.

**Conflicts of Interest:** The authors declare no conflict of interest. The funders had no role in the design of the study, in the collection, analyses, or interpretation of data, in the writing of the manuscript, or in the decision to publish the results.

## References

1. Sun, E.S. The metallogenic regularity of the silver deposits in the Manzhouli-Xinbaerhuyouqi metallogenic belt, Inner Mongolia. *Geol. Explor. Non-Ferr. Met.* **1995**, *4*, 23–29.
2. Zhu, H.-C.; Zhang, J.-F.; Quan, H.; Zhang, H.; Wang, H.-B. Metallogenic characteristics of nonferrous and noble metals in Ergun region. *J. Precious Met. Geol.* **1999**, *8*, 193–198.
3. Zhang, J.-F.; Wang, X.-Z.; Quan, H.; Wu, G.; Zhu, H.C. The forming conditions of nonferrous and precious metal deposits in the north of Derbugan metallogenic province. *Geol. Resour.* **2002**, *11*, 43–52.
4. Jia, B.; Liu, G.X.; Zhang, C.-H.; Yang, H.-Z.; Zhang, C.-P. Metallogenesis of the lead-zinc deposits controlled by the Mesozoic volcanic-subvolcanic rocks in Daxinganling region. *Geol. Resour.* **2012**, *21*, 114–121.
5. Xu, Z.-T.; Liu, Y.; Sun, J.-G.; Liang, X.-L.; Xu, Z.-K. Nature and ore formation of the Erdaohezi Pb-Zn deposit in the Great Xing'an Range, NE China. *Ore Geol. Rev.* **2020**, *119*, 103385. [[CrossRef](#)]
6. Qin, K.Z.; Wang, D.P.; Wang, Z.T.; Sun, S. Types, geological background, metallogenic provinces and ore-forming systematics of major copper deposits in eastern China. *Miner. Depos.* **1999**, *18*, 359–371.
7. Mao, J.-W.; Xie, G.-Q.; Zhang, Z.-H.; Li, X.-F.; Wang, Y.-T.; Zhang, C.-Q.; Li, Y.-F. Mesozoic large-scale metallogenic pulses in North China and corresponding geodynamic settings. *Acta Petrol. Sin.* **2005**, *21*, 169–188.
8. Pirajno, F. *Hydrothermal Processes and Mineral Systems*; Springer: Berlin, Germany, 2009.
9. Catchpole, H.; Kouzmanov, K.; Bendežú, A.; Ovtcharova, M.; Spikings, R.; Stein, H.; Fontboté, L. Timing of porphyry (Cu-Mo) and base metal (Zn-Pb-Ag-Cu) mineralisation in a magmatic-hydrothermal system—Morococha district, Peru. *Miner. Depos.* **2015**, *50*, 895–922. [[CrossRef](#)]
10. Li, J.-W.; Liang, Y.-W.; Wang, X.-Y.; Zhang, B.; Yang, Y.-C.; She, H.-Q.; Guo, Z.-J. The origin of the Erdaohezi lead-zinc deposit, Inner Mongolia. *J. Jilin Univ. (Earth Sci. Ed.)* **2011**, *41*, 1745–1754.
11. Zhao, Y.; Lü, J.-C.; Zhang, D.-B.; Zhou, Y.-H.; Shao, J.; Wang, B. Rb-Sr isochron age of Derbur Pb-Zn-Ag deposit in Erguna massif of northeast Inner Mongolia and its geological significance. *Miner. Depos.* **2017**, *36*, 893–904.
12. Li, T.-G.; Wu, G.; Liu, J.; Hu, Y.-Q.; Zhang, Y.-F.; Luo, D.-F. Rb-Sr isochron age of the Jiawula Pb-Zn-Ag deposit in the Manzhouli area and its geological significance. *Acta Petrol. Sin.* **2014**, *30*, 257–270.
13. Cavalcante, C.; Hollanda, M.-H.; Vauchez, A.; Kawata, M. How long can the middle crust remain partially molten during orogeny? *Geology* **2018**, *46*, 839–842. [[CrossRef](#)]
14. Jahn, B.-M.; Windley, B.; Natal'in, B.; Dobretsov, N. Phanerozoic continental growth in Central Asia. *J. Asian Earth Sci.* **2004**, *5*, 599–603. [[CrossRef](#)]
15. Pan, G.; Xiao, Q.; Lu, S.; Deng, J.; Feng, Y.; Zhang, K.; Zhang, Z.; Wang, F.; Xing, G.; Hao, G. Subdivision of tectonic units in China. *Geol. China* **2009**, *36*, 1–28.
16. Zhang, Z.; Institute of Inner Mongolia Tenth Geological Mineral Exploration. *General Survey Report of Lead Zinc Deposits in I and II Ore Blocks of the Qiyimuchang Mining Area, Chenba'erhu Country, Inner Mongolia*; Inner Mongolia Geology & Mineral Technology Co.: Inner Mongolia, China, 2005.
17. Duan, M.-X.; Ren, Y.-S.; Hou, Z.-S.; Sun, D.-Y.; Sun, Z.-M.; Qin, C.-J. Ore-forming fluid and ore genesis of the Biliya valley lead-zinc (silver) deposit in Erguna region, Inner Mongolia. *Mineral. Petrol.* **2014**, *2*, 60–67.
18. Duan, M.-X.; Ren, Y.-S.; Guo, H.-Y.; Wang, B.-C.; Zhao, X.-D.; Cai, Y.-L. Ore-forming fluids and genesis of Qiyimuchang lead-zinc deposit in Erguna area, Inner Mongolia. *Geol. Resour.* **2017**, *6*, 0557–0563.
19. Zheng, C.; Zhou, J.; Jin, W.; Ji, J.; Zhang, X.; Ma, Z.; Ding, X. Geochronology in the north segment of the Derbugan fault zone, Great Xing'an Range, NE China. *Acta Petrol. Sin.* **2009**, *25*, 1989–2000.
20. Zhao, W.-Z.; Zhang, Y.; Du, S.-W.; Zhang, B.-B.; Li, S.-K. Study on pretreatment of geological samples by ICP-MS method. *Chem. Eng.* **2018**, *269*, 25–28.
21. Liu, X.; Gao, S.; Yuan, H.-L.; Hattendorf, B.; Günther, D. Analysis of 42 major and trace elements in glass standard reference materials by 193 nm LA-ICPMS. *Acta Petrol. Sin.* **2002**, *18*, 408–418.
22. Liu, Z.; Shao, Y.; Zhou, X.; Zhang, Y.; Zhou, G. Hydrogen, oxygen, sulfur and lead isotope composition tracing for the ore-forming material source of Dongguashan copper (gold) deposit in Tongling, Anhui Province. *Acta Petrol. Sin.* **2014**, *30*, 199–208.
23. Li, Z.-S.; Zhang, C.-X.; Shu, L.; Shan, L.; Chi, N.-J.; Li, F.-C.; Wang, J.-L.; Yang, H. U-Pb dating of LA-MC-ICP-MS in situ of single zircon. *Shandong Land Resour.* **2022**, *38*, 71–81.
24. Xu, G.; Bian, Q.; Wang, Y. Tectonic evolution and metallization of the Erguna orogenic belt. *Chin. J. Geol.* **1998**, *33*, 84–92.
25. Sun, S.-S.; McDonough, W.F. Chemical and isotopic systematics of oceanic basalts: Implications for mantle composition and processes. *Geol. Soc. Lond. Spec. Publ.* **1989**, *42*, 313–345. [[CrossRef](#)]
26. Yin, Z.; Zhang, Y.; Yang, X.; Zhao, H.; Han, Z. Characteristics of Mesozoic volcanic rocks and magma evolution in northern Daxinganling. *Glob. Geol.* **2006**, *25*, 120–128.
27. Rollison, H.R. *Petrogeochemistry*; China University of Science and Technology Press: Hefei, China, 2000.
28. Shan, L.; Zheng, Y.-Y.; Xu, R.-K.; Cao, L.; Zhang, L.; Lian, Y.-L.; Lian, Y.-L. Review on sulfur isotopic tracing and hydrothermal metallogenesis. *Geol. Resour.* **2009**, *18*, 197–203.
29. Li, Y.; Lü, Z.; Yan, G.; Zhen, S.; Du, Z. Isotopic characteristics of S, Pb, H and O of Jiama copper polymetallic ore deposit, Tibet and their significance. *Earth Sci. Front* **2012**, *19*, 72–81.



30. Zhai, D.; Liu, J.; Wang, J.; Yao, M.; Liu, X.; Liu, Z.; Wu, S.; Fu, C.; Wang, S.; Li, Y. A study of stable isotope geochemistry of the Jiawula large Pb–Zn–Ag ore deposit, Inner Mongolia. *Earth Sci. Front.* **2013**, *20*, 213–225.
31. Zhang, B. *The Geological Features and Genesis of the Dongjun Lead-Zinc-Silver Deposit in Inner Mongolia, China*; Chinese Academy of Geological Sciences: Beijing, China, 2011.
32. Du, Q. *Duobaoshan Porphyry Copper Deposit*; Geology Press: Beijing, China, 1988.
33. Lu, Y. GeoKit-A geochemical toolkit for Microsoft Excel. *Geochimica* **2004**, *33*, 459–464.
34. Li, Y.; Zhao, Y.-Y. Lead isotopes in the sulfide ores from the Shesuo and Lawu copper deposits, northern Xizang. *Sediment. Geol. Tethyan Geol.* **2014**, *34*, 96–105.
35. Wu, Y.; Zheng, Y. Genesis of zircon and its constraints on interpretation of U–Pb age. *Chin. Sci. Bull.* **2004**, *49*, 1554–1569. [[CrossRef](#)]
36. Li, C. A review on the minerageny and situ microanalytical dating techniques of zircons. *Geol. Surv. Res.* **2009**, *33*, 161–174.
37. Li, C.-N. *Trace Element Petrology of Igneous Rocks*; China University of Geosciences Press: Wuhan, China, 1992; Volume 195.
38. Sun, C.-Y. *Crustal Growth and Reworking Processes of the Erguna and Xing'an Massifs: Evidence from Granitoids*; Jilin University: Jilin, China, 2021.
39. Gou, J. *Geochronology, Petrogenesis and Tectonic Setting of Mesozoic Volcanic Rocks, Southern Manzhouli Area, Inner Mongolia*; Jilin University: Jilin, China, 2013.
40. Zhang, Y.T. Geochemistry of Tamulangou Formation volcanic rocks in Mohe, North Da Hinggan Mountains. *Sci. Technol. Rev.* **2013**, *31*, 25–30.
41. Yang, B.; Chen, Z.L.; Zhang, Q.; Zhou, Z.J.; Han, F.B.; Zhang, W.G.; Ma, J.; Zhang, T. Geological characteristics and sulfur and lead isotopes of the Kanling lead-zinc deposit, Southern Tianshan Mountains. *Geol. China* **2018**, *45*, 155–167.
42. Cao, G.; Gao, T.; Wu, Y. Isotope and REE geochemistry of Puziwan Gold deposit, Shanxi. *China. Geol. Geochem.* **2000**, *28*, 10–14.
43. Basuki, N.I.; Taylor, B.E.; Spooner, E.T.C. Sulfur Isotope Evidence for Thermochemical Reduction of Dissolved Sulfate in Mississippi Valley-Type Zinc-Lead Mineralization, Bongara Area, Northern Peru. *Econ. Geol.* **2008**, *103*, 783–799. [[CrossRef](#)]
44. Chaussidon, M.; Lorand, J.-P. Sulphur isotope composition of orogenic spinel lherzolite massifs from Ariege (North-Eastern Pyrenees, France): An ion microprobe study. *Geochim. Cosmochim. Acta* **1990**, *54*, 2835–2846. [[CrossRef](#)]
45. Han, Y.W.; Ma, Z.D.; Zhang, H.F.; Zhang, B.R.; Li, W.L.; Gao, S.; Bao, Z.Y. *Geochemistry*; Geology Press: Beijing, China, 2003.
46. Jiang, S.-H.; Nie, F.-J.; Liu, Y.-F.; Yun, F. Sulfur and lead isotopic compositions of Bairendaba and Weilasituo silver-polymetallic deposits, Inner Mongolia. *Miner. Depos.* **2010**, *29*, 101–112.
47. Doe, B.R.; Stacey, J.S. The Application of Lead Isotopes to the Problems of Ore Genesis and Ore Prospect Evaluation: A Review. *Econ. Geol.* **1974**, *69*, 757–776. [[CrossRef](#)]
48. Zartman, R.E.; Doe, B.R. Plumbotectonics—The model. *Tectonophysics* **1981**, *75*, 135–162. [[CrossRef](#)]
49. Doe, B.R.; Zartman, R.E. Plumbotectonics, the Phanerozoic. In *Geochemistry of Hydrothermal Ore Deposits*, 2nd ed.; Barnes, H.L., Ed.; John Wiley: London, UK, 1979; pp. 22–70.
50. Isotope Geology Laboratory of Yichang Institute of Geology and Mineral Resources. *The Basic Problem of Lead Isotope Geology*; Geological Publishing House: Beijing, China, 1979.
51. Zhu, B.-Q.; Li, S.-H.; Dai, T.-M.; Chen, Y.-W.; Fan, S.-K.; Gui, X.-T.; Wang, H.-F. *Isotopes System Theory and Its Application in Earth Science-on the Evolution of the Continental Crust and Mantle*; Science Press: Beijing, China, 1998; pp. 216–235.
52. Li, T.; Wu, G.; Liu, J.; Wang, G.; Hu, Y.; Zhang, Y.; Luo, D.; Mao, Z.; Xu, B. Geochronology, fluid inclusions and isotopic characteristics of the Chaganbulagen Pb–Zn–Ag deposit, Inner Mongolia, China. *Lithos* **2016**, *261*, 340–355. [[CrossRef](#)]
53. Xu, Z.T. *Ore Genesis and Geodynamic Background of Lead-zinc Polymetallic Deposits in Erguna Area, Inner Mongolia*; Jilin University: Jilin, China, 2020.
54. Yang, Y.-C.; Guo, M.-J.; Wang, E.-J.; She, H.-Q.; Li, J.-W.; Zhang, B. Rb–Sr dating of sphalerites from Dongjun Pb–Zn–Ag deposit, Inner Mongolia and its geological significance. *Earth Sci. Front.* **2015**, *22*, 348.
55. Ren, J.; Niu, B.; Liu, Z. Soft collision, superposition orogeny and polycyclic suturing. *Earth Sci. Front.* **1999**, *6*, 85–93.
56. Tian, S.-L.; Jin, L.-F.; Shuang, B. The relationship between vein type Ag (Pb–Zn) deposits and volcanic rocks of the Tamulangou Formation in the Ergun Ore belt. *Geol. Explor. Non-Ferr. Met.* **1995**, *4*, 334–340.
57. Wu, F.-Y.; Sun, D.-Y.; Ge, W.-C.; Zhang, Y.-B.; Grant, M.L.; Wilde, S.A.; Jahn, B.-M. Geochronology of the Phanerozoic granitoids in northeastern China. *J. Asian Earth Sci.* **2011**, *41*, 1–30. [[CrossRef](#)]
58. Yu, J.-J.; Wang, F.; Xu, W.-L.; Gao, F.-H.; Pei, F.-P. Early Jurassic mafic magmatism in the Lesser Xing'an–Zhangguangcai Range, NE China, and its tectonic implications: Constraints from zircon U–Pb chronology and geochemistry. *Lithos* **2012**, *142*, 256–266. [[CrossRef](#)]
59. Guo, P.; Xu, W.-L.; Yu, J.-J.; Wang, F.; Tang, J.; Li, Y. Geochronology and geochemistry of Late Triassic bimodal igneous rocks at the eastern margin of the Songnen–Zhangguangcai Range Massif, Northeast China: Petrogenesis and tectonic implications. *Int. Geol. Rev.* **2015**, *58*, 196–215. [[CrossRef](#)]
60. Wang, F.; Xu, Y.-G.; Xu, W.-L.; Yang, L.; Wu, W.; Sun, C.-Y. Early Jurassic calc-alkaline magmatism in northeast China: Magmatic response to subduction of the Paleo-Pacific Plate beneath the Eurasian continent. *J. Asian Earth Sci.* **2017**, *143*, 249–268. [[CrossRef](#)]
61. Wang, Z.-H.; Ge, W.-C.; Yang, H.; Bi, J.-H.; Ji, Z.; Dong, Y.; Xu, W.-L. Petrogenesis and tectonic implications of Early Jurassic volcanic rocks of the Raohe accretionary complex, NE China. *J. Asian Earth Sci.* **2017**, *134*, 262–280. [[CrossRef](#)]

62. Xu, W.; Sun, C.; Tang, J.; Luan, J.; Wang, F. Basement nature and tectonic evolution of the Xing'an-Mongolian Orogenic Belt. *Earth Sci.* **2019**, *44*, 1620–1646.
63. Zorin, Y.A. Geodynamics of the western part of the Mongolia–Okhotsk collisional belt, Trans-Baikal region (Russia) and Mongolia. *Tectonophysics* **1999**, *306*, 33–56. [[CrossRef](#)]
64. Donskaya, T.; Gladkochub, D.; Mazukabzov, A.; Ivanov, A. Late Paleozoic–Mesozoic subduction-related magmatism at the southern margin of the Siberian continent and the 150 million-year history of the Mongol–Okhotsk Ocean. *J. Asian Earth Sci.* **2013**, *62*, 79–97. [[CrossRef](#)]
65. Fritzell, E.; Bull, A.; Shephard, G. Closure of the Mongol–Okhotsk Ocean: Insights from seismic tomography and numerical modelling. *Earth Planet. Sci. Lett.* **2016**, *445*, 1–12. [[CrossRef](#)]
66. Chen, Z.; Zhang, L.; Lu, B.; Li, Z.; Wu, H.; Xiang, P.; Huang, S. Geochronology and geochemistry of the Taipingchuan copper–molybdenum deposit in Inner Mongolia, and its geological significances. *Acta Petrol. Sinica* **2010**, *26*, 1437–1449. [[CrossRef](#)]
67. Jiang, S.-H.; Nie, F.-J.; Su, Y.-J.; Bai, D.-M.; Liu, Y.-F. Geochronology and origin of the Erdenet superlarge Cu–Mo deposit in Mongolia. *Diqiu Xuebao (Acta Geosci. Sin.)* **2010**, *31*, 289–306.
68. Lü, Z.-C.; Duan, G.-Z.; Hao, L.-B.; Li, D.-C.; Dong, G.-H. The interaction system between Mesozoic tectonic, fluid, petrogenesis and mineralization in the northeast of the Northern Orogenic Belt, China. *Geotecton. Et Metallog.* **2010**, *25*, 161–170.
69. She, H.-Q.; Li, J.-W.; Xiang, A.-D.; Guan, J.-D.; Yang, Y.-C.; Zhang, D.-Q.; Tan, G.; Zhang, B. U–Pb ages of the zircons from primary rocks in middle-northern Daxinganling and its implications to geotectonic evolution. *Acta Petrol. Sin.* **2012**, *28*, 571–594.
70. Xu, W.-L.; Pei, F.-P.; Wang, F.; Meng, E.; Ji, W.-Q.; Yang, D.-B.; Wang, W. Spatial–temporal relationships of Mesozoic volcanic rocks in NE China: Constraints on tectonic overprinting and transformations between multiple tectonic regimes. *J. Asian Earth Sci.* **2013**, *74*, 167–193. [[CrossRef](#)]
71. Li, Y.; Xu, W.-L.; Wang, F.; Tang, J.; Sun, C.-Y.; Wang, Z.-J. Early–Middle Ordovician volcanism along the eastern margin of the Xing'an Massif, Northeast China: Constraints on the suture location between the Xing'an and Songnen–Zhangguangcai Range massifs. *Int. Geol. Rev.* **2018**, *60*, 2046–2062. [[CrossRef](#)]
72. Meng, E.; Xu, W.; Yang, D.; Qiu, K.; Li, C.; Zhu, H. Zircon U–Pb chronology, geochemistry of Mesozoic volcanic rocks from the Lingquan basin in Manzhouli area, and its tectonic implications. *Acta Petrol. Sin.* **2011**, *27*, 1209–1226.
73. Wang, J.; He, Z.; Xu, W. Petrogenesis of riebeckite rhyolites in the southern Da Hinggan Mts.: Geochronological and geochemical evidence. *Acta Petrol. Sin.* **2013**, *29*, 853–863.
74. Tang, J.; Xu, W.; Wang, F.; Ge, W. Subduction history of the Paleo-Pacific slab beneath Eurasian continent: Mesozoic–Paleogene magmatic records in Northeast Asia. *Sci. China Earth Sci.* **2018**, *61*, 527–559. [[CrossRef](#)]
75. Mao, A.Q. *Magmatic Rocks of Mesozoic Volcanic Basins in Central Erguna Block: Petrogenesis and Geodynamics*; Jilin University: Jilin, China, 2020.